QCD Corrections to Higgs Pair Production in Bottom Quark Fusion

Sally Dawson[a], Chung Kao[b,c], Yili Wang[c] and Peter Williams[c]

[a]*Department of Physics,*
Brookhaven National Laboratory,
Upton, NY 11973, USA
[b]*Fermi National Accelerator Laboratory,*
P.O. Box 500,
Batavia, Illinois 60510, USA
[c]*Homer L. Dodge Department of Physics and Astronomy,*
University of Oklahoma,
Norman, Oklahoma 73019, USA

Abstract

We present a complete next-to-leading order (NLO) calculation for the total cross section of inclusive Higgs pair production via bottom-quark fusion ($b\bar{b} \to hh$) at the CERN Large Hadron Collider (LHC) in the Standard Model. The NLO QCD corrections lead to less dependence on the renormalization scale (μ_R) and the factorization scale (μ_F) than the leading-order (LO) cross section, and they significantly increase the LO cross section. The rate for inclusive Higgs pair production is small in the Standard Model, but can be large in models with enhanced couplings of the b quark to the Higgs bosons.

I. INTRODUCTION

In the Standard Model (SM), one Higgs doublet is responsible for the electroweak symmetry breaking (EWSB) that generates masses for gauge bosons and fermions. A neutral Higgs boson (h) remains after EWSB, and it is the only SM elementary particle that has not been observed in high energy experiments. In extensions of the Standard Model, there can be more Higgs bosons.

One of the most important goals of the Fermilab Tevatron Run II and the CERN Large Hadron Collider (LHC) is to discover the Higgs bosons or to prove their non-existence. The present lower bound on the standard Higgs boson mass from direct searches at LEP2 [1, 2] is $M_h > 114$ GeV. The electroweak precision measurements set an upper limit of $M_h < 166$ GeV at 95% confidence level for the Standard Model Higgs boson [3] using the recently measured top quark mass of $m_t = 171.4 \pm 1.2 \pm 1.8$ GeV [4]. This limit increases to 199 GeV when the LEP2 direct search limit is included.

The Fermilab Tevatron and the LHC will play crucial roles in Higgs searches. Once a candidate Higgs boson is discovered, it will be necessary to determine the Higgs couplings and spin to see if the Higgs candidate has the properties of the SM Higgs boson. One of the most difficult properties to measure is the trilinear self coupling of a Higgs boson [5, 6, 7, 8, 9]. The high energy and high luminosity at the LHC might provide opportunities to detect a pair of Higgs bosons as well as a discovery channel to measure the trilinear Higgs couplings in the SM and in models with more Higgs bosons. In the Standard Model, gluon fusion is the dominant process to produce a pair of Higgs bosons via triangle and box diagrams with internal top quarks and bottom quarks [10, 11, 12, 13]. Bottom quark fusion can also produce Higgs pairs at a lower rate.

At tree level, the physical production mechanism for a Higgs boson pair in association with b quarks is $gg \to b\bar{b}hh$. This process contains a large collinear logarithm from the gluon splitting into a collinear $b\bar{b}$ pair, $\Lambda \equiv \ln(M_h/m_b)$. These logarithms can be resummed by using a perturbatively defined b quark parton distribution function (PDF) which is inherently $O(\alpha_s\Lambda)$ [14, 15, 16, 17]. In this approach, the ordering of perturbation theory is changed to be an expansion in $\mathcal{O}(\alpha_s)$ and Λ^{-1}.

When using a scheme with b quark PDFs for Higgs pair production in association with b quarks, the leading order (LO) process becomes $b\bar{b} \to hh$, and we compute the NLO cross section with $O(\alpha_s)$ and $O(1/\Lambda)$ corrections to this process. The subprocess $bg \to bhh$ is a correction of $O(1/\Lambda)$ to the lowest order process, while $gg \to b\bar{b}hh$ is $O(1/\Lambda^2)$.

The rate for Higgs pair production at the LHC is small in the SM. However, it can become significant in models in which the Higgs coupling to the bottom quark is enhanced [18]. In two Higgs doublet models with Model II type of Yukawa interactions (including the minimal supersymmetric standard model (MSSM)), the ratio of the Higgs vacuum expectation values ($\tan\beta \equiv v_2/v_1$) is an important parameter. A large value of $\tan\beta$ greatly enhances the Higgs coupling with bottom quarks and makes bottom quark fusion become the largest production mechanism for producing a Higgs boson at the LHC. The D0 experiment has placed limits on single Higgs production in association with b quarks for large values of $\tan\beta$ [19].

In this paper, we present the complete next-to-leading order (NLO) calculations to the production of Higgs pairs via bottom quark fusion in the Standard Model. We compute a consistent set of $O(\alpha_s)$ and $O(1/\Lambda)$ corrections. In a future paper, we will present results for double Higgs production at NLO in the MSSM [20].

The theoretical prediction depends on the number of b quarks tagged. Here, we consider

only inclusive processes in which there are no tagged b quarks. We apply the two cutoff phase space slicing method [21, 22] to calculate corrections from real gluon emission. Two arbitrary small parameters are introduced to split the phase space in real gluon emission into soft, hard/collinear, and hard/non-collinear regions. The production in the hard/non-collinear region is finite and can be calculated numerically. Divergences are isolated into soft and hard/collinear regions. The soft (infrared) singularities cancel with the infrared singularities in the virtual corrections. The collinear singularities are absorbed into the initial parton distribution functions.

In section II, we compute the leading-order cross section for $pp \to hh + X$ via $b\bar{b} \to hh$. In section III, we provide a complete next-leading order (NLO) calculation for hh production. At the parton level, we compute one-loop virtual corrections and real gluon emission corrections to $b\bar{b} \to hh$ and the $\mathcal{O}(1/\Lambda)$ subleading process, $bg \to bhh$. The associated production, $gg \to b\bar{b}hh$, is finite and is a subleading correction of $\mathcal{O}(1/\Lambda^2)$ to the inclusive rate for $pp \to hh + X$. We use MadGraph [23] and HELAS [24] to compute its LO production rate with a finite mass of the bottom quark. Numerical results are given in Section IV and conclusions are drawn in section V. In addition, there is an appendix to present formulas for the b quark running mass.

II.   LEADING-ORDER CROSS SECTION FOR $b\bar{b} \to hh$

The leading order (LO) inclusive cross section for $pp \to hh + X$ via $b\bar{b} \to hh$ is evaluated with

$$\sigma_{LO} = \int dx_1 dx_2 \left[b(x_1)\bar{b}(x_2) + \bar{b}(x_1)b(x_2) \right] \hat{\sigma}_{LO}(s, t, u)(b\bar{b} \to hh) \tag{1}$$

where $b(x)$ and $\bar{b}(x)$ are the LO parton distribution functions for bottom quarks in the proton, $\hat{\sigma}_{LO}(s, t, u)$ is the parton level cross section for $b\bar{b} \to hh$ and s, t, u are the Mandelstam variables. Fig. 1 shows the tree level Feynman diagrams for $b\bar{b} \to hh$.
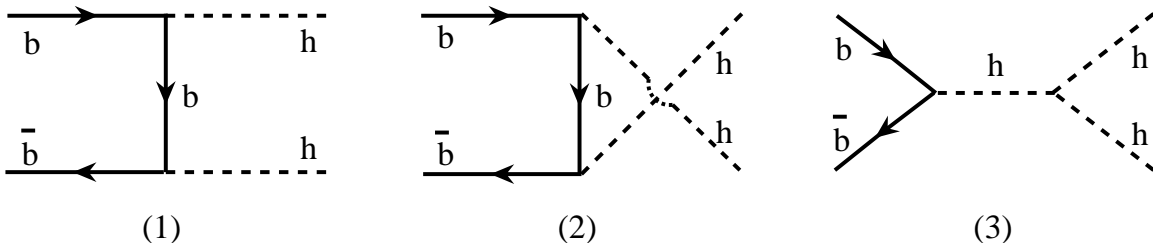

FIG. 1: The lowest order Feynman diagrams for $b\bar{b} \to hh$.

We assign momenta to the initial and the final state particles with

$$b(p_1)\bar{b}(p_2) \to h(p_3)h(p_4)$$

and $p_1 + p_2 = p_3 + p_4$. We take the $b\bar{b}h$ and hhh couplings to be $-i\frac{m_b}{v}C_{bh}$ and $-i3\frac{M_h^2}{v}C_{hhh}$, respectively, with $v =$ the Higgs vacuum expectation value $\simeq 246$ GeV, $C_{bbh} = 1$ and $C_{hhh} = 1$ in the Standard Model. We evaluate the bottom quark mass in the $hb\bar{b}$ Yukawa coupling by using the $\overline{MS}$ mass, $\bar{m}_b(\mu)$ (defined in Appendix A), for a two-loop heavy

quark running mass [25] with $m_b(\text{pole}) = 4.7$ GeV and the NLO evolution of the strong coupling [26].

In addition, the Mandelstam variables are defined as

$$
\begin{aligned}
s &= (p_1 + p_2)^2 \\
t &= (p_1 - p_3)^2 \\
u &= (p_2 - p_3)^2 \quad .
\end{aligned}
$$

Following the simplified ACOT prescription [27, 28, 29], we take $m_b = 0$ everywhere except in the Yukawa couplings. Then the tree level amplitudes of the s, t and u channels are:

$$
\begin{aligned}
M_s^0 &\equiv \hat{M}_s^0 \delta_{ji} = -\frac{3 C_{bh} C_{hhh} \bar{m}_b(\mu) M_h^2}{v^2 \left(s - M_h^2 + i M_h \Gamma_h\right)} \delta_{ji} \bar{v}(p_2) u(p_1) \\
M_t^0 &\equiv \hat{M}_t^0 \delta_{ji} = \frac{C_{bh}^2 \bar{m}_b^2(\mu)}{v^2 t} \delta_{ji} \bar{v}(p_2) \slashed{p}_3 u(p_1) \\
M_u^0 &\equiv \hat{M}_u^0 \delta_{ji} = -\frac{C_{bh}^2 \bar{m}_b^2(\mu)}{v^2 u} \delta_{ji} \bar{v}(p_2) \slashed{p}_3 u(p_1)
\end{aligned}
$$

where i and j are color indices for initial b and $\bar{b}$ quarks. The μ parameter is an arbitrary mass, which is introduced such that both the renormalized strong coupling and Yukawa coupling are dimensionless in N dimensions. The corresponding spin- and color-averaged matrix elements squared including interference terms are

$$
\begin{aligned}
\langle |M_s^0|^2 \rangle &= \frac{3}{2} \left(\frac{\bar{m}_b^2(\mu)}{v^2}\right) C_{bh}^2 C_{hhh}^2 \frac{s}{v^2} \left|\frac{M_h^2}{s - M_h^2 + i \Gamma_h M_h}\right|^2 \\
\langle |M_t^0|^2 \rangle &= \frac{1}{6} \left(\frac{\bar{m}_b^4(\mu)}{v^4}\right) C_{bh}^4 \left(\frac{u}{t} - \frac{M_h^4}{t^2}\right) \\
\langle |M_u^0|^2 \rangle &= \frac{1}{6} \left(\frac{\bar{m}_b^4(\mu)}{v^4}\right) C_{bh}^4 \left(\frac{t}{u} - \frac{M_h^4}{u^2}\right) \\
\langle Re(M_t^0 \bar{M}_u^0) \rangle &= -\frac{1}{6} \left(\frac{\bar{m}_b^4(\mu)}{v^4}\right) C_{bh}^4 \left(1 - \frac{M_h^4}{tu}\right) \quad ,
\end{aligned}
$$

where Γ_h is the decay width of the Higgs boson.

Summing the above terms, we obtain the total matrix element squared

$$
\begin{aligned}
\langle |M_0|^2 \rangle &= \langle |M_s^0|^2 \rangle + \langle |M_t^0|^2 \rangle + \langle |M_u^0|^2 \rangle + 2 \langle Re(M_t^0 \overline{M}_u^0) \rangle \\
&= \frac{1}{6} \left(\frac{\bar{m}_b^2(\mu)}{v^2}\right) C_{bh}^2 \left[9 \frac{s}{v^2} C_{hhh}^2 \left|\frac{M_h^2}{s - M_h^2 + i M_h \Gamma_h}\right|^2 \right. \\
&\quad \left. + \left(\frac{\bar{m}_b^2(\mu)}{v^2}\right) C_{bh}^2 \left(1 - \frac{M_h^4}{ut}\right) \frac{(u - t)^2}{ut}\right] \quad .
\end{aligned}
$$

The parton level cross section for inclusive $b\bar{b} \to hh$ production becomes

$$
\hat{\sigma}_{\text{LO}} = \int \frac{1}{2s} \frac{1}{2} \langle |M_0|^2 \rangle d\Phi_2(b\bar{b} \to hh) \tag{2}
$$

where $d\Phi_2(b\bar{b} \to hh)$ denotes the two-body phase space factor and a factor of $1/2$ comes from identical particles in the final state.

4

III.   NEXT-TO-LEADING ORDER CORRECTIONS FOR $b\bar{b} \rightarrow hh$

To determine the next-to-leading order (NLO) corrections for Higgs boson pair production in bottom quark fusion, we evaluate the cross section for (a) the leading-order subprocess ($b\bar{b} \rightarrow hh$), (b) the α_s corrections, and (c) the $1/\Lambda$ corrections ($bg \rightarrow bhh$), where $\Lambda \equiv \ln(M_h/m_b)$. The order α_s corrections have contributions from one-loop diagrams with virtual gluons ($b\bar{b} \rightarrow hh$) and tree-level real gluon emission ($b\bar{b} \rightarrow hhg$). The NLO correction contains both the α_s and the $1/\Lambda$ corrections.

We write the parton level NLO cross section as

$$\begin{aligned}
\hat{\sigma}_{\text{NLO}}(x_1, x_2, \mu) &= \hat{\sigma}_{\text{LO}}(x_1, x_2, \mu) + \delta\hat{\sigma}_{NLO}(x_1, x_2, \mu) \\
\delta\hat{\sigma}_{\text{NLO}}(x_1, x_2, \mu) &= \delta\hat{\sigma}_{\alpha_s}(x_1, x_2, \mu) + \delta\hat{\sigma}_{1/\Lambda}(x_1, x_2, \mu)
\end{aligned} \quad (3)$$

where $\hat{\sigma}_{\text{LO}}(x_1, x_2, \mu)$ is the leading order (Born) cross section and $\delta\hat{\sigma}_{\text{NLO}}(x_1, x_2, \mu)$ is the next-to-leading order correction to the Born cross section, $x_{1,2}$ are the momentum fractions of the partons, $x_1 x_2 = \hat{s}/S$, S is the center of mass energy of the hadrons and $\mu = \mu_R$ is the renormalization scale.

The $\mathcal{O}(\alpha_s)$ correction includes contributions from both virtual and real gluon emission:

$$\delta\hat{\sigma}_{\alpha_s}(x_1, x_2, \mu) = \delta\hat{\sigma}_v(x_1, x_2, \mu) + \delta\hat{\sigma}_r(x_1, x_2, \mu) \quad (4)$$

where $\delta\hat{\sigma}_v(x_1, x_2, \mu)$ and $\delta\hat{\sigma}_r(x_1, x_2, \mu)$ represent virtual and real gluon emission NLO corrections to $b\bar{b} \rightarrow hh$.

A.   Corrections with virtual gluons

The one-loop diagrams for the $\mathcal{O}(\alpha_s)$ corrections to $b\bar{b} \rightarrow hh$ are shown in Fig. 2. The α_s corrections involving virtual gluons are evaluated as the interferences between Born diagrams (Fig. 1) and one-loop virtual diagrams (Fig. 2).

$$|M_v|^2 = M_0 \overline{M}_{loop} + M_{loop} \overline{M}_0 = 2Re(M_{loop}\overline{M}_0) \, .$$

We evaluate the amplitudes of the one-loop diagrams by applying dimensional regularization in N dimensions with $N \equiv 4 - 2\epsilon$. The virtual diagrams are computed analytically and all tensor integrals are reduced to linear combinations of one-loop scalar functions. All amplitudes for the virtual corrections can be reduced to Born amplitudes multiplied by coefficients X_i. We find,

$$2Re(M_{loop}\overline{M}_0) = 2C_F g_s^2 Re\{\left[X_s|M_s^0|^2 + X_t|M_t^0|^2 + X_u|M_u^0|^2 + (X_t + X_u)Re(M_t^0\overline{M_u^0})\right]\} \quad (5)$$

where $C_F = 4/3$ and

$$\begin{aligned}
X_s &\equiv X_9 \\
X_t &\equiv X_1 + X_3 + X_5 + X_7 \\
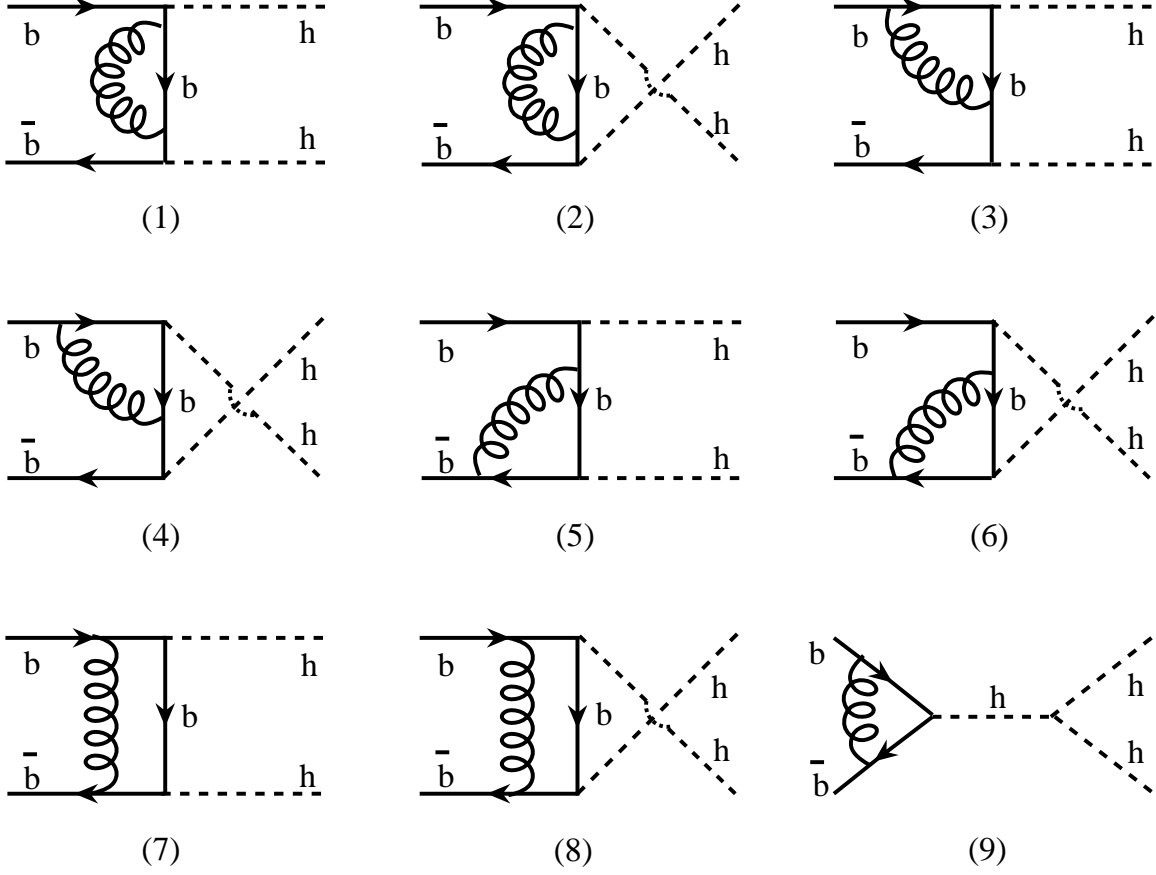X_u &\equiv X_2 + X_4 + X_6 + X_8
\end{aligned}$$

FIG. 2: One-loop virtual corrections to $b\bar{b} \to hh$.

The coefficients are,

$$X_1 = -A\left(\frac{1}{\epsilon} + 1 - \ln(-t)\right)$$

$$X_2 = -A\left(\frac{1}{\epsilon} + 1 - \ln(-u)\right)$$

$$X_3 = X_5 = 2A\left\{(-t)^{-\epsilon}\left(\frac{1}{\epsilon} + 2\right) - \left(\frac{M_h^2}{M_h^2 - t}\right)\left[\frac{1}{\epsilon}\ln\left(\frac{-t}{M_h^2}\right) + \frac{1}{2}\ln^2(M_h^2) - \frac{1}{2}\ln^2(-t) - \frac{\pi^2}{2}\right] - 1\right\}$$

$$X_4 = X_6 = 2A\left\{(-u)^{-\epsilon}\left(\frac{1}{\epsilon} + 2\right) - \left(\frac{M_h^2}{M_h^2 - u}\right)\left[\frac{1}{\epsilon}\ln\left(\frac{-u}{M_h^2}\right) + \frac{1}{2}\ln^2(M_h^2) - \frac{1}{2}\ln^2(-u) - \frac{\pi^2}{2}\right] - 1\right\}$$

$$X_7 = 2A\left\{-\frac{1}{\epsilon^2} + \frac{1}{\epsilon}\left[\frac{2M_h^2}{M_h^2 - t}\ln\left(\frac{-t}{M_h^2}\right) + \ln(s)\right] + F(t)\right\}$$

$$X_8 = 2A\left\{-\frac{1}{\epsilon^2} + \frac{1}{\epsilon}\left[\frac{2M_h^2}{M_h^2 - u}\ln\left(\frac{-u}{M_h^2}\right) + \ln(s)\right] + F(u)\right\}$$

$$X_9 = -2A\left[\frac{1}{\epsilon^2} - \frac{1}{\epsilon}\ln(s) + \frac{1}{2}\ln^2(s) + 1 - \frac{2\pi^2}{3}\right] \quad , \tag{6}$$

where A is a normalization factor

$$A = \frac{1}{16\pi^2}\Gamma(1+\epsilon)(4\pi\mu^2)^\epsilon.$$

The function $F(x)$ is defined as

$$
\begin{aligned}
F(x) &= \frac{-x}{M_h^2 - x}\left[-\ln^2(M_h^2) + \ln^2(-x) + \pi^2\right] \\
&+ \frac{x}{s\beta_h}\left[\ln\left(\frac{M_h^2}{s}\right)\ln\left(\frac{1-\beta_h}{1+\beta_h}\right) + 2Li_2\left(\frac{1+\beta_h}{2}\right) - 2Li_2\left(\frac{1-\beta_h}{2}\right)\right] \\
&- 2\ln^2\left(\frac{-x\sqrt{s}}{M_h^2}\right) - 4Li_2\left(1 - \frac{x}{M_h^2}\right) + \frac{2\pi^2}{3}
\end{aligned}
\tag{7}
$$

where $\beta_h = \sqrt{1 - 4M_h^2/s}$ and Li_2 is the dilogarithm or the Spence function [30].

The virtual corrections contain both ultraviolet (UV) and infrared (IR) divergences. In the $\overline{MS}$ scheme, the b quark Yukawa coupling is renormalized with the counter term [31]

$$
\frac{\delta m_b}{m_b} = -A\frac{16\pi\alpha_s}{\epsilon} \quad .
$$

This counter term contributes to the total matrix element squared by

$$
\begin{aligned}
|M_{CT}|^2 &= 2\frac{\delta m_b}{m_b}|M_s^0|^2 + 4\frac{\delta m_b}{m_b}\left(|M_t^0|^2 + |M_u^0|^2 + 2Re(M_t^0\overline{M_u^0})\right) \\
&= -\frac{32A\pi\alpha_s}{\epsilon}\left[|M_s^0|^2 + 2(|M_t^0|^2 + |M_u^0|^2 + 2ReM_t^0\overline{M_u^0})\right] \quad .
\end{aligned}
$$

Summing over all relevant contributions, we obtain the following expression for the one-loop virtual corrections

$$
\begin{aligned}
|M_v|^2 &= 2Re(M_{loop}\overline{M_0}) + |M_{CT}|^2 \\
&= |M_0|^2\left\{A\frac{64\pi\alpha_s}{3}\left[-\frac{1}{\epsilon^2} + \frac{1}{\epsilon}\ln(s) - \frac{3}{2\epsilon}\right]\right\} + A\frac{64\pi\alpha_s}{3}|M_D|^2 \quad ,
\end{aligned}
\tag{8}
$$

where $|M_D|^2$ contains the finite terms:

$$
\begin{aligned}
|M_D|^2 &= \left[-\frac{1}{2}\ln^2(s) + \frac{2\pi^2}{3} - 1\right]|M_s^0|^2 \\
&+ \frac{M_h^2}{M_h^2 - t}\left[-\ln^2(M_h^2) + \ln^2(-t) + \pi^2\right]|M_t^0|^2 + \left[F(t) + \frac{3}{2} - \frac{3}{2}\ln(-t)\right]|M_t^0|^2 \\
&+ \frac{M_h^2}{M_h^2 - u}\left[-\ln^2(M_h^2) + \ln^2(-u) + \pi^2\right]|M_u^0|^2 + \left[F(u) + \frac{3}{2} - \frac{3}{2}\ln(-u)\right]|M_u^0|^2 \\
&+ \frac{M_h^4}{(M_h^2 - t)(M_h^2 - u)}\left[\ln^2(-t) + \ln^2(-u) + F(t) + F(u)\right. \\
&\left. - \frac{3}{2}\ln(-t) - \frac{3}{2}\ln(-u) + 2\pi^2 + 3\right]Re(M_t^0\overline{M_u^0}) \\
&+ \frac{M_h^2}{(M_h^2 - t)(M_h^2 - u)}\left\{-s\ln^2(M_h^2) - u\ln^2(-t) - t\ln^2(-u)\right. \\
&\left. - \left[F(t) + F(u) - \frac{3}{2}\ln(-t) - \frac{3}{2}\ln(-u) + \pi^2 + 3\right](t+u)\right\}Re(M_t^0\overline{M_u^0}) \\
&+ \frac{tu}{(M_h^2 - t)(M_h^2 - u)}\left[F(t) + F(u) + 3 - \frac{3}{2}\ln(-t) - \frac{3}{2}\ln(-u)\right]Re(M_t^0\overline{M_u^0}) \quad .
\end{aligned}
\tag{9}
$$

The divergences left in Eq. 8 are infrared divergences which are canceled by the infrared divergences in the real gluon emission corrections discussed in the next subsection.

B. Real gluon emission

The Feynman diagrams for real gluon emission ($b\bar{b} \to hhg$) are shown in Fig. 3. We assign the momentum as

$$b(p_1)\bar{b}(p_2) \to h(p_3)h(p_4)g(p_g).$$

The real gluon emission corrections have infrared (IR) and collinear singularities. The infrared singularities cancel the virtual infrared singularities in Eq. 8 and the collinear singularities are absorbed into parton distribution functions. We apply the two cut-off phase space slicing (PSS) method [21, 22] to isolate these singularities in different regions of phase space.

We introduce two small cutoffs to split the phase space in the real gluon emission process. First, we introduce a soft cutoff (δ_s) to separate the phase space of the process $b\bar{b} \to hhg$ into *soft* and *hard* regions according to the emitted gluon energy. The soft region is the region where the radiated gluon energy satisfies $E_g < \delta_s \frac{\sqrt{s}}{2}$, while the hard region is the region where the gluon energy satisfies, $E_g \geq \delta_s \frac{\sqrt{s}}{2}$. Then the contributions from real gluon emission can be decomposed as

$$\hat{\sigma}_r = \hat{\sigma}_{soft} + \hat{\sigma}_{hard} . \tag{10}$$

Although the energy of the emitted gluon in the hard region is above the threshold, there still exist singularities when the emitted gluon is parallel to one of the initial bottom quarks. We introduce a collinear cutoff (δ_c) to isolate this collinear singularity. The phase space in the hard region is decomposed into hard/collinear and hard/non-collinear regions. In the hard/collinear portion, the gluon is emitted within an angle satisfying

$$\frac{2p_1 \cdot p_g}{E_g \sqrt{s}} < \delta_c \quad or \quad \frac{2p_2 \cdot p_g}{E_g \sqrt{s}} < \delta_c \quad . \tag{11}$$

The parton level cross section in the hard region is split into hard/collinear and hard/noncollinear regions,

$$\hat{\sigma}_{hard} = \hat{\sigma}_{hard/c} + \hat{\sigma}_{hard/nc} \quad , \tag{12}$$

where $\hat{\sigma}_{hard/c}$ is obtained by integrating over the hard/collinear region of the gluon phase space. It includes the collinear singularities and can be evaluated analytically in N dimensions. The hard non-collinear cross section ($\hat{\sigma}_{hard/nc}$) is finite. We have calculated $\hat{\sigma}_{hard/c}$ and $\hat{\sigma}_{hard/nc}$ numerically with a collinear cutoff (δ_c). The analytic matrix elements squared are used in our calculations for α_s and $1/\Lambda$ corrections. Since δ_s and δ_c are arbitrary cut-offs, the dependence of the cross section on δ_s and δ_c is not physical and cancels in the total NLO cross section.

1. Soft gluons

The soft gluon emission amplitudes for the diagrams in Fig. 3 are obtained by setting the gluon momentum p_g to zero everywhere except in the denominators that are singular as $p_g \to 0$. The soft gluon emission corrections are

$$M_{soft} = g_s^2 T_{ji}^a \left(\frac{p_2^\mu}{p_2 \cdot p_g} - \frac{p_1^\mu}{p_1 \cdot p_g} \right) (\hat{M}_s^0 + \hat{M}_t^0 + \hat{M}_u^0) . \tag{13}$$
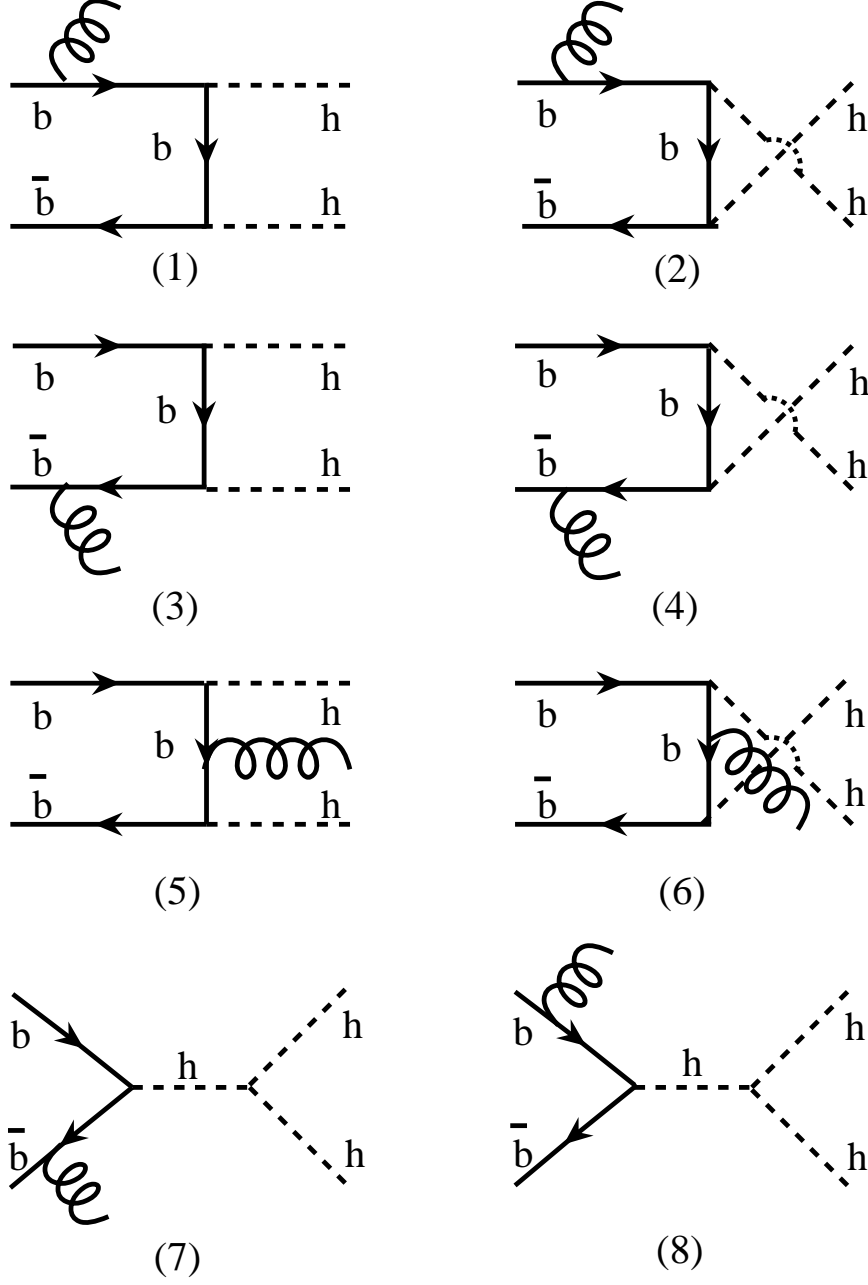
FIG. 3: Feynman diagrams for Higgs pair production in bottom quark fusion with real gluon emission ($b\bar{b} \rightarrow hhg$).

There is a logarithmic divergence in the integral of the matrix element squared over the soft three-body phase space. The three-body phase space in the soft gluon emission approximation is,

$$
\begin{aligned}
d\Phi_3|_{soft} &= \left[\frac{d^{N-1}p_3}{2E_3(2\pi)^{N-1}} \frac{d^{N-1}p_4}{2E_4(2\pi)^{N-1}} (2\pi)^N \delta^N(p_1 + p_2 - p_3 - p_4) \right] \frac{d^{N-1}p_g}{2E_g(2\pi)^{N-1}} \\
&= (d\Phi_2)(d\Phi_g|_{soft})
\end{aligned}
\tag{14}
$$

where $d\Phi_2$ is the two-body phase space factor and $d\Phi_g|_{soft}$ is the soft gluon phase space. In the center of mass frame of the incoming partons,

$$
\begin{aligned}
d\Phi_g|_{soft} &= \frac{d^{N-1}p_g}{(2\pi)^{N-1}2E_g} \\
&= \frac{\Gamma(1-\epsilon)}{\Gamma(1-2\epsilon)}\frac{\pi^\epsilon}{(2\pi)^3}\int_0^{\frac{\sqrt{s}}{2}\delta_s} dE_g E_g^{1-2\epsilon}\int_0^\pi d\theta_1 sin^{1-2\epsilon}\theta_1 \int_0^\pi d\theta_2 sin^{-2\epsilon}\theta_2 .
\end{aligned}
\tag{15}
$$

Together with the matrix element in the corresponding soft approximation, this integral can be evaluated analytically,

$$
\begin{aligned}
\langle|M'_{soft}|^2\rangle &\equiv \int d\Phi_g|_{soft}\langle|M_{soft}|^2\rangle \\
&= 4\pi\alpha_s\langle|M_0|^2\rangle C_F\frac{1}{4\pi^2\epsilon^2}\left(\frac{4\pi\mu^2}{\delta_s^2 s}\right)^\epsilon\frac{\Gamma(1-\epsilon)}{\Gamma(1-2\epsilon)} \\
&= \langle|M_0|^2\rangle A\frac{64\pi\alpha_s}{3}\left[\frac{1}{\epsilon^2} - \frac{1}{\epsilon}\ln(\delta_s^2) - \frac{1}{\epsilon}\ln(s) + \frac{1}{2}\ln^2(s\delta_s^2) - \frac{\pi^2}{3}\right] .
\end{aligned}
\tag{16}
$$

The divergences in Eq. 16 cancel the IR singularities in Eq. 8 of the virtual corrections. Adding Eq. 8 and Eq. 16 together we obtain

$$
\begin{aligned}
\langle|M_v|^2\rangle + \langle|M'_{soft}|^2\rangle &= \langle|M_0|^2\rangle\left\{A\frac{64\pi\alpha_s}{3}\left(-\frac{1}{\epsilon}\right)\left[\ln(\delta_s^2) + \frac{3}{2}\right]\right. \\
&\left. + A\frac{64\pi\alpha_s}{3}\left[\frac{1}{2}\ln^2(s\delta_s^2) - \frac{\pi^2}{3}\right]\right\} + A\frac{64\pi\alpha_s}{3}|M_D|^2 .
\end{aligned}
\tag{17}
$$

However, this equation still has a collinear singularity, which can be absorbed into the parton distribution functions. We discuss this collinear singularity in the next subsection.

2. Hard gluons

In the hard/collinear region, the hard gluon is emitted collinearly to one of the initial partons. The phase space is greatly simplified in the collinear limit. The initial-state b quark splits into a hard parton b' and a collinear hard gluon g by $b \rightarrow b'g$ with approximately $p_{b'} = zp_b$ and $p_g = (1-z)p_b$. In the hard/collinear limit, the matrix element squared for $b\bar{b} \rightarrow hhg$ factorizes into the Born matrix element squared and the Altarelli-Parisi splitting function for $b \rightarrow b'g$

$$
\langle\sum|M_{hard/c}|^2\rangle(b\bar{b}\rightarrow hhg) \rightarrow (4\pi\alpha_s)\langle\sum|M_0|^2\rangle\frac{-2P_{bb}(z,\epsilon)}{z(p_1-p_g)^2}(\mu^2)^\epsilon + (1\leftrightarrow 2) ,
\tag{18}
$$

where P_{bb} is the Altarelli-Parisi splitting function for $b \rightarrow b'g$ at the lowest order

$$
\begin{aligned}
P_{bb}(z,\epsilon) &= C_F\left[\frac{1+z^2}{1-z} - \epsilon(1-z)\right] \\
&= P_{bb}(z) + \epsilon P'_{bb}(z) .
\end{aligned}
\tag{19}
$$

10

The process can be factorized in two steps. First, one incoming b quark radiates a hard gluon and becomes b'. Then this b' collides with another incoming b quark to produce two Higgs bosons by $b'\bar{b} \to hh$. The hard/collinear phase space is,

$$d\Phi_3 \,|_{hard/c} = d\Phi_2(zp_1 + p_2 \to p_3 + p_4)\frac{d^{N-1}p_g}{(2\pi)^{N-1}2E_g} \ . \tag{20}$$

To carry out the integration over $d^{N-1}p_g$ in the collinear approximation, we introduce a new variable, $s_{bg} = 2p_1 \cdot p_g$, which is constrained by $0 \leq s_{bg} \leq \frac{s}{2}(1-z)\delta_c$. The hard/collinear phase space of the gluon becomes,

$$\frac{d^{N-1}p_g}{(2\pi)^{N-1}2E_g} \,|_{hard/c} = \frac{(4\pi)^\epsilon}{16\pi^2}\frac{1}{\Gamma(1-\epsilon)}dz\,ds_{bg}[(1-z)s_{bg}]^{-\epsilon} \ . \tag{21}$$

The ds_{bg} integral can be evaluated to find the cross section in the hard/collinear region,

$$
\begin{aligned}
\sigma_{hard/c} &= \int dx_1 dx_2 \, \bar{b}(x_2)\frac{\alpha_s}{2\pi}\frac{\Gamma(1-\epsilon)}{\Gamma(1-2\epsilon)}\left(\frac{4\pi\mu^2}{s}\right)^\epsilon(-\frac{1}{\epsilon})\delta_c^{-\epsilon}\int_{x_1}^{1-\delta_s}\frac{dz}{z}b(x_1/z)P_{bb}(z,\epsilon)\hat{\sigma}_{\mathrm{LO}} \\
&\times \left[\frac{(1-z)^2}{2}\right]^{-\epsilon} + (b \leftrightarrow \bar{b}) + (1 \leftrightarrow 2) \ .
\end{aligned}
\tag{22}
$$

This equation has collinear divergences which we remove by absorbing them into bare parton distribution functions. We introduce a modified (NLO) parton distribution function at the factorization scale μ_F in the $\overline{MS}$ scheme:

$$
\begin{aligned}
b(x) &= b(x,\mu_F)\left\{1 + \frac{2\alpha_s}{3\pi}(4\pi)^\epsilon\Gamma(1+\epsilon)\left(\frac{1}{\epsilon}\right)\left[\ln(\delta_s^2) + \frac{3}{2}\right]\right\} \\
&+ \frac{\alpha_s}{2\pi}\frac{\Gamma(1-\epsilon)}{\Gamma(1-2\epsilon)}(4\pi)^\epsilon\left(\frac{1}{\epsilon}\right)\int_x^{1-\delta_s}P_{bb}(z)\frac{dz}{z}b(x/z) \ .
\end{aligned}
\tag{23}
$$

Replacing $b(x)$ in the lowest order hadronic cross section by $b(x,\mu_F)$ and dropping terms higher than $\mathcal{O}(\alpha_s)$, we obtain the Born cross section that is proportional to α_s

$$
\begin{aligned}
\sigma_{\mathrm{Born}} &= \int dx_1 dx_2 b(x_1,\mu_F)\bar{b}(x_2,\mu_F)\hat{\sigma}_{LO}(x_1,x_2,\mu_R) \\
&+ \int dx_1 dx_2 b(x_1,\mu_F)\bar{b}(x_2,\mu_F)\hat{\sigma}_{LO}(x_1,x_2,\mu_R)\left\{\frac{4\alpha_s}{3\pi}(4\pi)^\epsilon\Gamma(1+\epsilon)\left(\frac{1}{\epsilon}\right)\left[\ln(\delta_s^2) + \frac{3}{2}\right]\right\} \\
&+ \left\{\int dx_1 dx_2 \bar{b}(x_2,\mu_F)\hat{\sigma}_{LO}(x_1,x_2,\mu_R)\frac{\alpha_s}{2\pi}\frac{\Gamma(1-\epsilon)}{\Gamma(1-2\epsilon)}(4\pi)^\epsilon\left(\frac{1}{\epsilon}\right)\right. \\
&\times \left.\int_{x_1}^{1-\delta_s}P_{bb}(z)\frac{dz}{z}b(x_1/z,\mu_F) + (b \leftrightarrow \bar{b})\right\} \\
&+ (1 \leftrightarrow 2) \ .
\end{aligned}
\tag{24}
$$

The $1/\epsilon$ poles in the second line cancel the collinear singularities of the soft gluon corrections in Eq. 17, while the divergences in the third line cancel with the hard/collinear divergences in Eq. 22. These cancellations leave a finite cross section that has dependence on μ_R and μ_F.

The remaining region has hard/non-collinear gluons and yields a finite contribution to the cross section. We compute this contribution numerically.

C. Corrections from $bg \to bhh$

Now let us consider the contributions from the parton subprocess $bg \to bhh$, which is an $\mathcal{O}(1/\Lambda)$ correction to the LO process of $b\bar{b} \to hh$. In calculating this cross section, again we ignore the bottom quark mass, m_b, except in the Yukawa couplings where the running mass is used. There are no IR singularities in the $bg \to bhh$ subprocess. However, when we integrate over the momenta of the b quarks, there are initial state collinear singularities which arise from gluon splitting to a pair of collinear b quarks. These singularities are absorbed into gluon parton distribution functions.
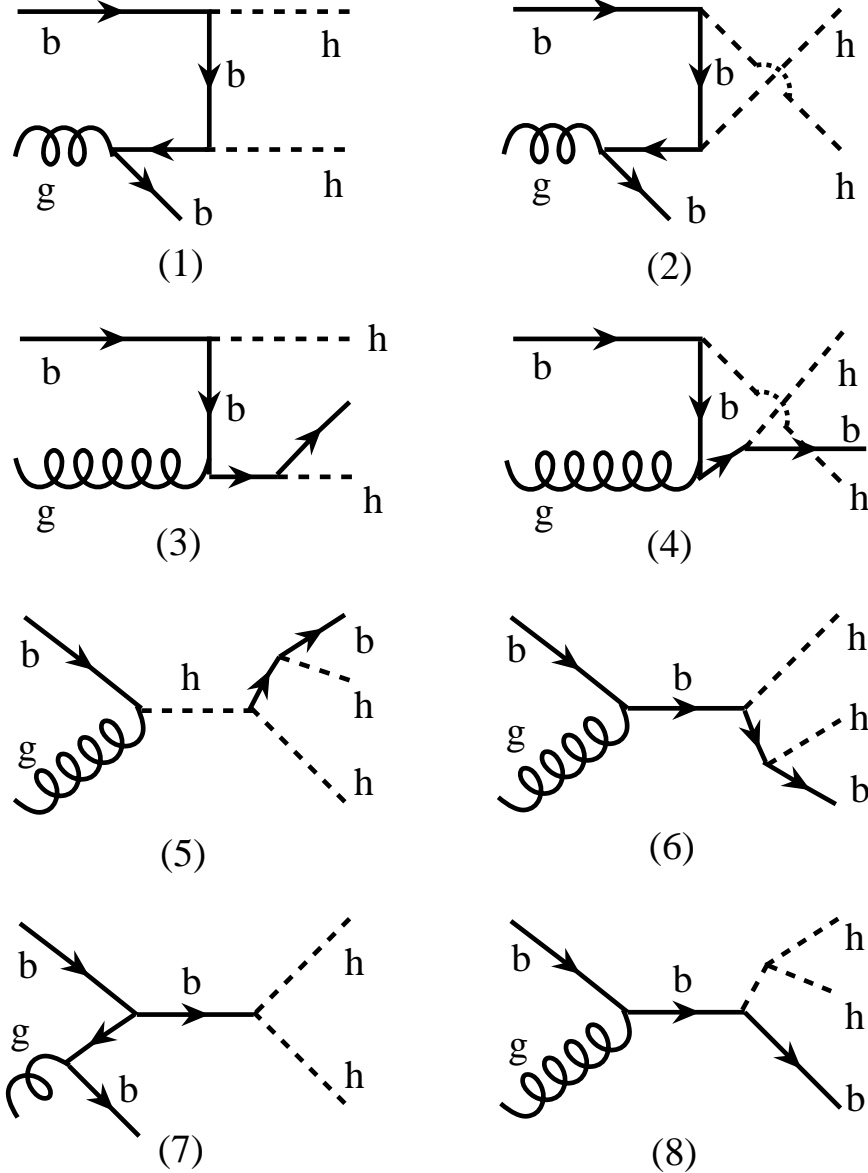

FIG. 4: The lowest order Feynman diagrams for $bg \to bhh$.

The eight diagrams for the $bg \to bhh$ subprocess are shown in Fig. 4. We assign momenta to partons as

$$b(p_1)g(p_2) \to b(p_b)h(p_3)h(p_4) \quad .$$

As there are no IR divergences, we do not need to separate the final b quark phase space into soft and hard regions. The cross section is:

$$\sigma_{bg} = \int dx_1 dx_2 b(x_1) g(x_2) \hat{\sigma}(bg \to bhh) + (1 \leftrightarrow 2) \quad . \tag{25}$$

As shown in diagrams (1), (2) and (7) of Fig. 4, the initial gluon can be considered to split into two b quarks. When these two b quarks are parallel to each other, collinear singularities appear. To remove these collinear singularities, we introduce a collinear cutoff (δ_c) to split the final b quark phase space into collinear and non-collinear regions. In the collinear region, the final b is emitted within an angle satisfying,

$$\frac{-(p_2 - p_b)^2}{E_b \sqrt{s}} < \delta_c \quad . \tag{26}$$

Using the same method as for the $b\bar{b} \to hhg$ real gluon emission corrections, we find the cross section in the collinear region:

$$\sigma_c = \int dx_1 dx_2 \, b(x_1) \hat{\sigma} \frac{\alpha_s}{2\pi} \frac{\Gamma(1-\epsilon)}{\Gamma(1-2\epsilon)} \left(\frac{4\pi\mu^2}{s} \right)^{\epsilon} (-\frac{1}{\epsilon}) \delta_c^{-\epsilon}$$
$$\times \int_{x_2}^{1} \frac{dz}{z} g(x_2/z) P_{bg}(z,\epsilon) \left[\frac{(1-z)^2}{2z} \right]^{-\epsilon} \quad . \tag{27}$$

P_{bg} is the Altarelli-Parisi splitting function for $g \to bb'$ at lowest order,

$$P_{bg}(z,\epsilon) = \frac{1}{2} \left[z^2 + (1-z)^2 \right] - \epsilon z (1-z)$$
$$= P_{bg}(z) + \epsilon P'_{bg}(z) \quad . \tag{28}$$

Again we introduce a modified parton distribution function,

$$g(x, \mu_F) = g(x) + \frac{\alpha_s}{2\pi} \frac{\Gamma(1-\epsilon)}{\Gamma(1-2\epsilon)} (4\pi)^{\epsilon} \left(-\frac{1}{\epsilon} \right) \int_x^1 P_{bg}(z) \frac{dz}{z} g(x/z) \tag{29}$$

The contribution to the NLO total cross section from the bg initial state is then,

$$\delta\sigma_{NLO}^{bg} = \sigma_c + \sigma_{nc}$$
$$= \frac{\alpha_s}{2\pi} \int dx_1 dx_2 \int_{x_2}^{1} \frac{dz}{z} \hat{\sigma}_{LO} \, b(x_1, \mu_F) g(x_2/z, \mu_F)$$
$$\times \left[\frac{z^2 + (1-z)^2}{2} \ln \left(\frac{s}{\mu^2} \frac{(1-z)^2}{z} \frac{\delta_c}{2} \right) + z(1-z) \right]$$
$$+ \int dx_1 dx_2 \, b(x_1, \mu_F) g(x_2, \mu_F) \hat{\sigma}_{nc}(bg \to bhh) + (1 \leftrightarrow 2) \quad . \tag{30}$$

Here $\hat{\sigma}_{LO}$ is the Born cross section for $b\bar{b} \to hh$ and $\hat{\sigma}_{nc}$ is the Born cross section for $bg \to bhh$. The $\bar{b}g \to \bar{b}hh$ process has exactly the same contribution as $bg \to bhh$.

D. Next-to-leading order cross section for $b\bar{b} \to hh$

We have obtained the virtual and the real gluon emission $\mathcal{O}(\alpha_s)$ corrections to $b\bar{b} \to hh$. The real gluon emission corrections include three regions: soft, hard/collinear and hard/non-collinear. The total next-to-leading order cross section can now be assembled from the lowest order cross section, the virtual corrections, and the real gluon emission corrections. Summing all of the above pieces, we obtain the $\mathcal{O}(\alpha_s)$ next-to-leading-order cross section corrections,

$$
\begin{aligned}
\sigma_{\text{Born}} + \delta\sigma_{\alpha_s} &= \sigma_{\text{Born}} + \sigma_v + \sigma_{soft} + \sigma_{hard/c} + \sigma_{hard/nc} \\
&= \int dx_1 dx_2 \quad b(x_1, \mu)\bar{b}(x_2, \mu) \left\{ \hat{\sigma}_{LO} \left[1 - \frac{4\alpha_s}{3\pi} \ln(\mu^2) \left(\ln(\delta_s^2) + \frac{3}{2} \right) \right] + \hat{\sigma}_{finite} \right\} \\
&+ \frac{\alpha_s}{2\pi} C_F \int dx_1 dx_2 \int_{x_1}^{1-\delta_s} \frac{dz}{z} \hat{\sigma}_{LO} \left[b(x_1/z, \mu)\bar{b}(x_2, \mu) + b(x_2, \mu)\bar{b}(x_1/z, \mu) \right] \\
&\times \left[\frac{1+z^2}{1-z} \ln\left(\frac{s}{\mu^2} \frac{(1-z)^2}{z} \frac{\delta_c}{2} \right) + 1 - z \right] \\
&+ \int dx_1 dx_2\, b(x_1, \mu)\bar{b}(x_2, \mu) \hat{\sigma}_{hard/nc}(b\bar{b} \to hhg) \\
&+ (1 \leftrightarrow 2)
\end{aligned}
\tag{31}
$$

where $\hat{\sigma}_{finite}$ represents the finite cross section with contributions from both virtual and soft gluon radiative corrections,

$$
\hat{\sigma}_{finite} = \int \frac{1}{2s} \frac{1}{2} \frac{4\alpha_s}{3\pi} \left\{ \left[\frac{1}{2} \ln^2(s\delta_s^2) - \frac{\pi^2}{3} \right] |M_0|^2 + |M_D|^2 \right\} d\Phi_2(b\bar{b} \to hh) .
\tag{32}
$$

We have taken $\mu = \mu_R = \mu_F$.

The $\mathcal{O}(1/\Lambda)$ corrections from the subprocesses $bg \to bhh$ and $\bar{b}g \to \bar{b}hh$ include collinear and non-collinear contributions and yield the $1/\Lambda$ corrections for Higgs pair production associated with one b quark.

$$
\delta\sigma_{1/\Lambda} = \delta\sigma_{NLO}^{bg} + \delta\sigma_{NLO}^{\bar{b}g}
\tag{33}
$$

Summing Eq. 31 and 33, we get the total next-to-leading-order cross section for Higgs pair production from bottom quark fusion,

$$
\sigma_{NLO} = \sigma_{\text{Born}} + \delta\sigma_{\alpha_s} + \delta\sigma_{1/\Lambda} .
\tag{34}
$$

The associated Higgs boson pair production with $b\bar{b}$ occurs via gluon fusion $gg \to b\bar{b}hh$ and quark-antiquark annihilation $q\bar{q} \to b\bar{b}hh$. These are subleading corrections to the NLO results given above. To estimate the cross section from these subprocesses, we have applied a nonzero value of $m_b = 4.7$ GeV for the bottom quark mass except in the Yukawa couplings where the running mass is used. We use MadGraph [23] and HELAS [24] to calculate the cross sections for these processes and find that the contribution from $q\bar{q} \to b\bar{b}hh$ is much smaller than that from $gg \to b\bar{b}hh$.

IV. RESULTS FOR HIGGS PAIR PRODUCTION IN BOTTOM QUARK FUSION

In this section, we present our results for the next-to-leading-order inclusive cross section for $pp \to hh + X$ via bottom quark fusion, $b\bar{b} \to hh$. We use the lowest order CTEQ6L1 parton distribution functions (PDFs) [32] at the factorization scale μ_F with the leading-order evolution of the strong coupling $\alpha_s(\mu_R)$ at the renormalization scale μ_R to calculate the LO cross section and the CTEQ6M PDFs at μ_F with the next-to-leading-order evolution of $\alpha_s(\mu_R)$ to evaluate the NLO inclusive cross section.
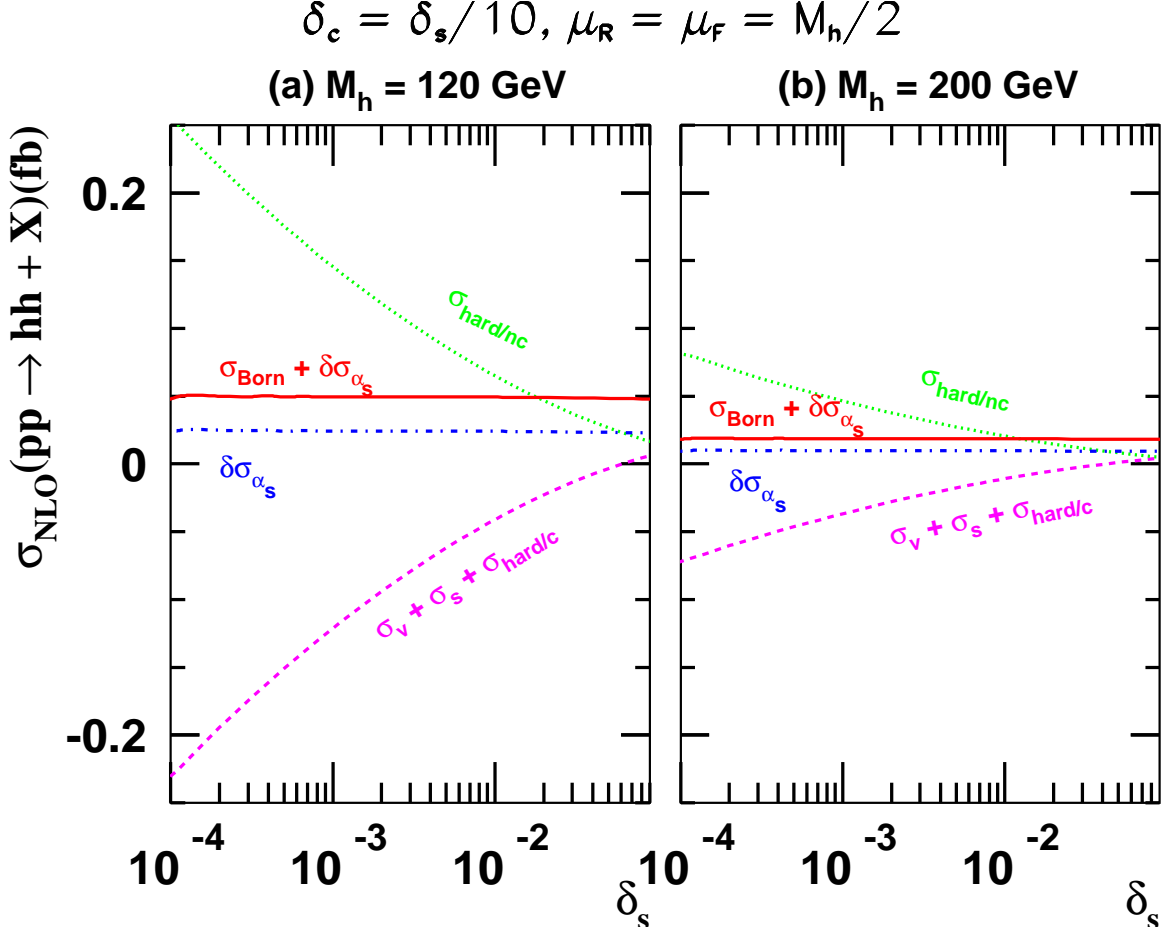

FIG. 5: Order α_s corrections $\delta\sigma_{\alpha_s}(b\bar{b} \to hh)$ (dash-dot, blue) versus the soft cutoff δ_s with $\sqrt{S} = 14$ TeV, $\mu_R = \mu_F = M_h/2$ and $\delta_c = \delta_s/10$ for (a) $M_h = 120$ GeV and (b) $M_h = 200$ GeV. These corrections have contributions from virtual gluons (σ_v), soft gluon emission (σ_s), hard/collinear gluon emission ($\sigma_{hard/c}$), and hard/non-collinear gluon emission ($\sigma_{hard/nc}$). These graphs show the cancellation of the δ_s dependence between $\sigma_v + \sigma_s + \sigma_{hard/c}$ (dash, magenta) and $\sigma_{hard/nc}$ (dot, green). Also shown is the sum of σ_{Born} and $\delta\sigma_{\alpha_s}$ (solid, red).

We have introduced two arbitrary small cutoffs, the soft cutoff δ_s and the collinear cutoff δ_c, to split the phase space in the real gluon emission corrections into soft, hard/collinear and hard/non-collinear regions. These separations are not physical and our final results are reliable only if they are not sensitive to these parameters.

To check the dependence of the $\mathcal{O}(\alpha_s)$ NLO cross section on these two parameters, we present the order α_s corrections for Higgs pair production $\delta\sigma_{\alpha_s}(b\bar{b} \to hh)$ versus δ_s in Fig. 5
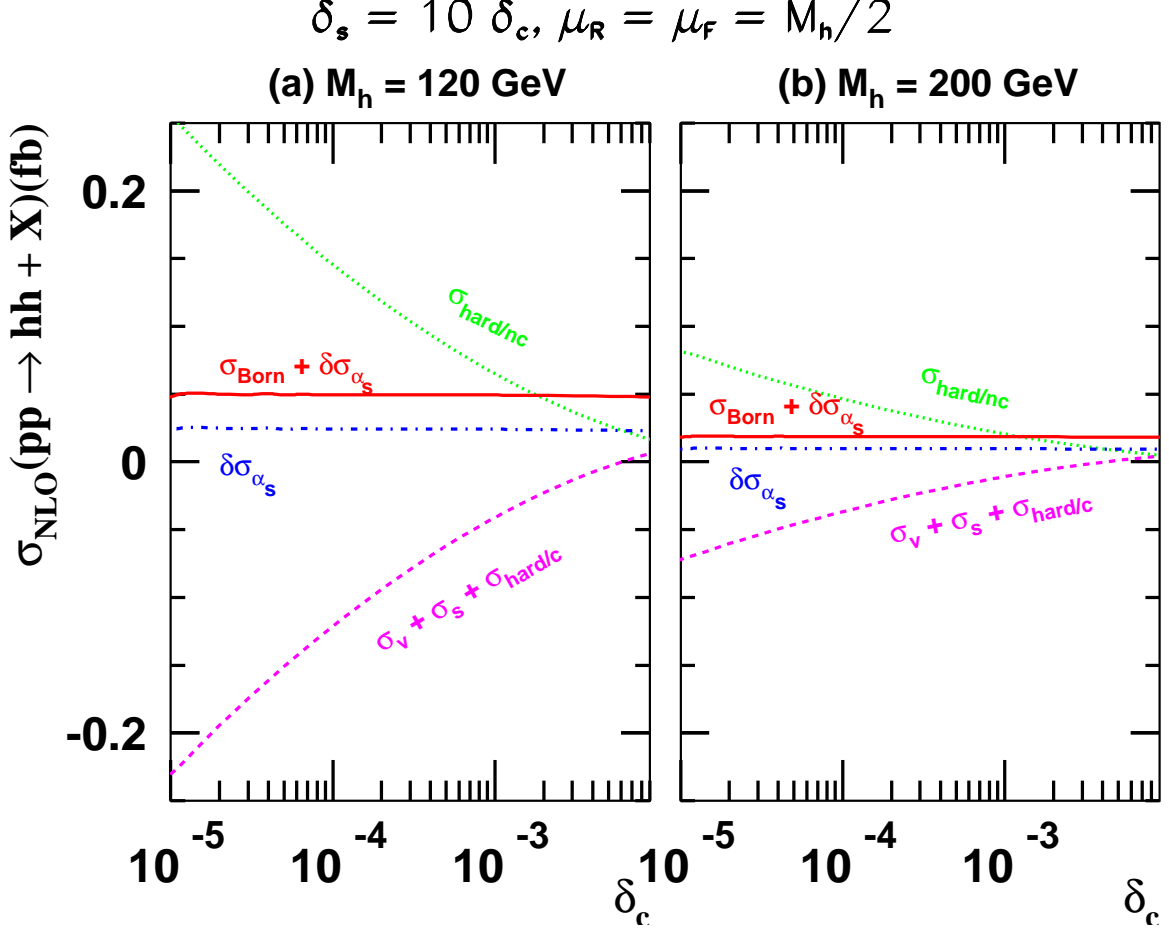
$$\delta_s = 10\,\delta_c,\ \mu_R = \mu_F = M_h/2$$

(a) $M_h = 120$ GeV   **(b) $M_h = 200$ GeV**

FIG. 6: Order α_s corrections $\delta\sigma_{\alpha_s}(b\bar{b} \to hh)$ (dash-dot, blue) versus the hard/collinear cutoff δ_c with $\sqrt{S} = 14$ TeV, $\mu_R = \mu_F = M_h/2$ and $\delta_s = 10\delta_c$ for (a) $M_h = 120$ GeV and (b) $M_h = 200$ GeV. These corrections have contributions from virtual gluons (σ_v), soft gluon emission (σ_s), hard/collinear gluon emission ($\sigma_{hard/c}$), and hard/non-collinear gluon emission ($\sigma_{hard/nc}$). These graphs show the cancellation of the δ_c dependence between $\sigma_v + \sigma_s + \sigma_{hard/c}$ (dash, magenta) and $\sigma_{hard/nc}$ (dot, green). Also shown is the sum of σ_{Born} and $\delta\sigma_{\alpha_s}$ (solid, red).

and $\delta\sigma_{\alpha_s}(b\bar{b} \to hh)$ versus δ_c in Fig. 6 with $\sqrt{S} = 14$ TeV for (a) $M_h = 120$ GeV and (b) $M_h = 200$ GeV. These corrections have contributions from virtual gluons (σ_v), soft gluon emission (σ_s), hard/collinear gluon emission ($\sigma_{hard/c}$), and hard/non-collinear gluon emission ($\sigma_{hard/nc}$). These graphs show the cancellation of the δ_s dependence and the δ_c dependence between $\sigma_v + \sigma_s + \sigma_{hard/c}$ and $\sigma_{hard/nc}$. Also shown is the sum of σ_{Born} and $\delta\sigma_{\alpha_s}$. We have chosen $\delta_c = \delta_s/10$ and the renormalization/factorization scales to be $\mu_F = \mu_R = M_h/2$.

There are several points to note.

- We divide the phase space of the real gluon emission correction into soft, hard/collinear and hard/non-collinear regions by introducing two small cut-offs δ_s and δ_c. The correction in each region is then integrated over the corresponding phase space. As we can see in these graphs, the corrections in each region are very sensitive to the values of δ_s and δ_c.

- Since these two small cutoffs, δ_s and δ_c, are arbitrary, the total cross section should

not depend on either one of them. These two figures show the cancellation of the δ_s and δ_c dependences.

- At the renormalization/factorization scale $\mu_R = \mu_F = M_h/2$, the $\mathcal{O}(\alpha_s)$ NLO cross section corrections are comparable with the Born cross section. This implies that the $\mathcal{O}(\alpha_s)$ corrections significantly increase the LO cross section.
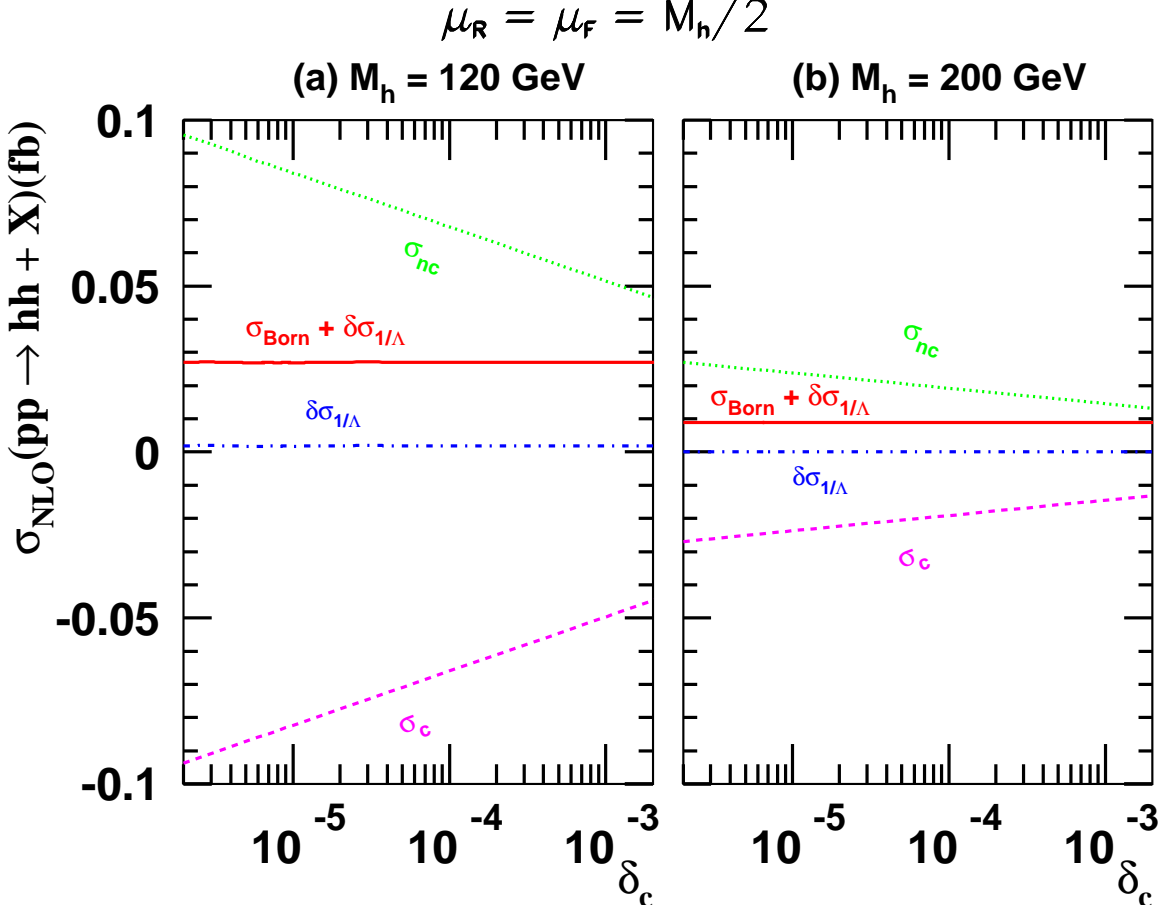

FIG. 7: Order $1/\Lambda$ corrections $\delta\sigma(1/\Lambda)(bg \to bhh)$ (dash-dot, blue) versus the collinear cutoff δ_c with $\sqrt{S} = 14$ TeV and $\mu_R = \mu_F = M_h/2$ for (a) $M_h = 120$ GeV and (b) $M_h = 200$ GeV. This figure shows the cancellation of the δ_c dependence between σ_c (dash, magenta) and σ_{nc} (dot, green). Also shown is the sum of σ_{Born} and $\delta\sigma_{1/\Lambda}$ (solid, red).

Figure 7 shows the independence of order $1/\Lambda$ corrections ($\delta\sigma_{1/\Lambda}$) on the collinear cutoff δ_c in the $bg \to bhh$ subprocess. Like the α_s corrections to $b\bar{b} \to hh$, the contributions from collinear and non-collinear regions are very sensitive to the values of δ_c, but the total $\mathcal{O}(1/\Lambda)$ NLO cross section correction is independent of δ_c. The $\mathcal{O}(1/\Lambda)$ contributions from $bg \to bhh$ are much smaller than the $\mathcal{O}(\alpha_s)$ NLO corrections from the $b\bar{b}$ initial state.

In Fig. 8, we study the dependence of the LO and NLO cross sections on the renormalization and factorization scales. We present the next-to-leading order cross section $\sigma_{\text{NLO}}(pp \to hh + X)$ via bottom quark fusion versus $\mu = \mu_R = \mu_F$ with $\delta_s = 10^{-3}$ and $\delta_c = 10^{-4}$ for (a) $M_h = 120$ GeV and (b) $M_h = 200$ GeV. Also shown are the LO
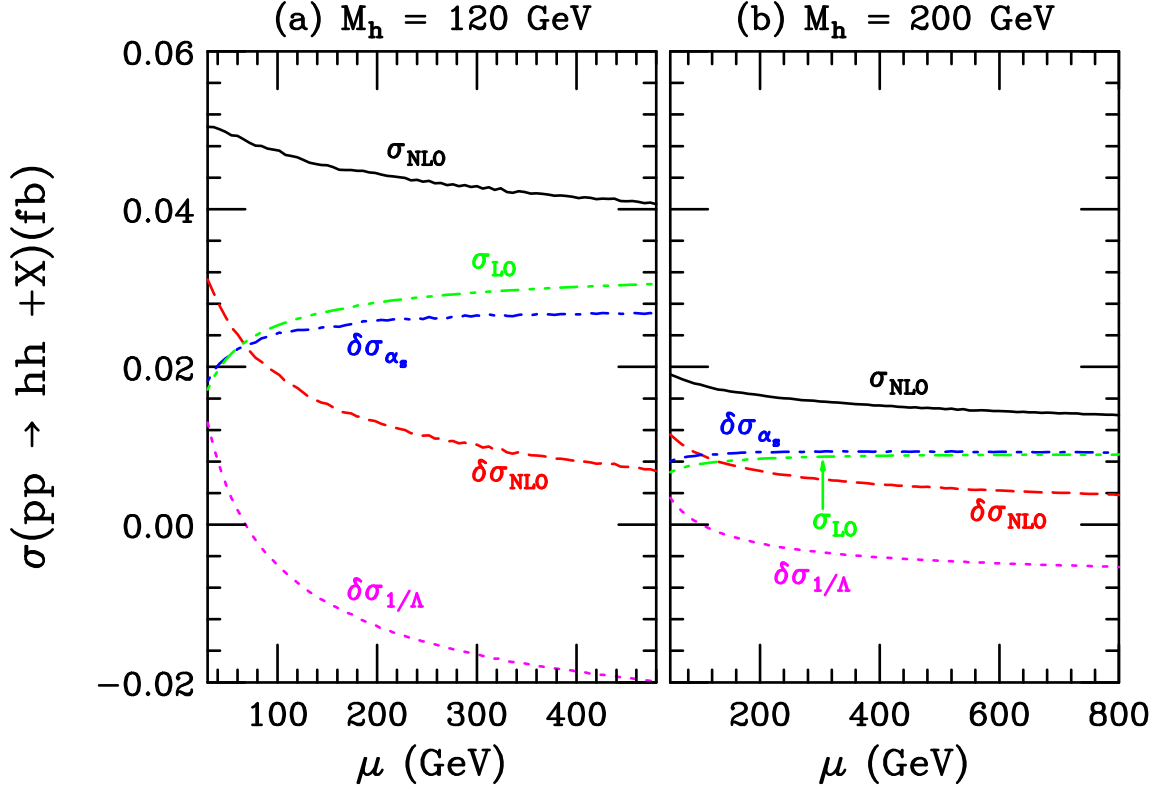
17

FIG. 8: Next-to-leading order cross section $\sigma_{NLO}(pp \to hh + X)$ (solid, black) in bottom quark fusion versus renormalization/factorization scale $\mu = \mu_R = \mu_F$ with $\sqrt{S} = 14$ TeV, $\delta_s = 10^{-3}$ and $\delta_c = 10^{-4}$, for (a) $M_h = 120$ GeV and (b) $M_h = 200$ GeV. Also shown are the LO cross section σ_{LO} (dash-dot-dot, green), α_s corrections $\delta\sigma_{\alpha_s}$ (dash-dot, blue), $1/\Lambda$ corrections $\delta\sigma_{1/\Lambda}$ (dot, magenta), and the NLO correction $\delta\sigma_{NLO} = \delta\sigma_{\alpha_s} + \delta\sigma_{1/\Lambda}$ (dash, red).

cross section (σ_{LO}), α_s corrections ($\delta\sigma_{\alpha_s}$), $1/\Lambda$ corrections ($\delta\sigma_{1/\Lambda}$), and the NLO correction $\delta\sigma_{NLO} = \delta\sigma_{\alpha_s} + \delta\sigma_{1/\Lambda}$.

We note that:

- The total NLO cross section corrections decrease with μ. The larger the Higgs mass, the slower the decrease of the NLO corrections.

- The NLO cross section has less dependence on the renormalization and factorization scales than does the LO cross section.

Fig. 9 shows the NLO total cross section $pp \to hh + X$ in bottom quark fusion as a function of the Higgs mass (M_h) at the LHC with $\sqrt{S} = 14$ TeV, $\delta_s = 10^{-3}$ and $\delta_c = 10^{-4}$. The renormalization and factorization scales are chosen to be (a) $\mu = M_h$ and (b) $\mu = M_h/2$. The NLO cross section correction for $\mu = M_h$ is bigger than for $\mu = M_h/2$. In addition, we present the LO cross section (σ_{LO}), α_s corrections ($\delta\sigma_{\alpha_s}$), $1/\Lambda$ corrections ($\delta\sigma_{1/\Lambda}$), and the NLO correction $\delta\sigma_{NLO} = \delta\sigma_{\alpha_s} + \delta\sigma_{1/\Lambda}$.
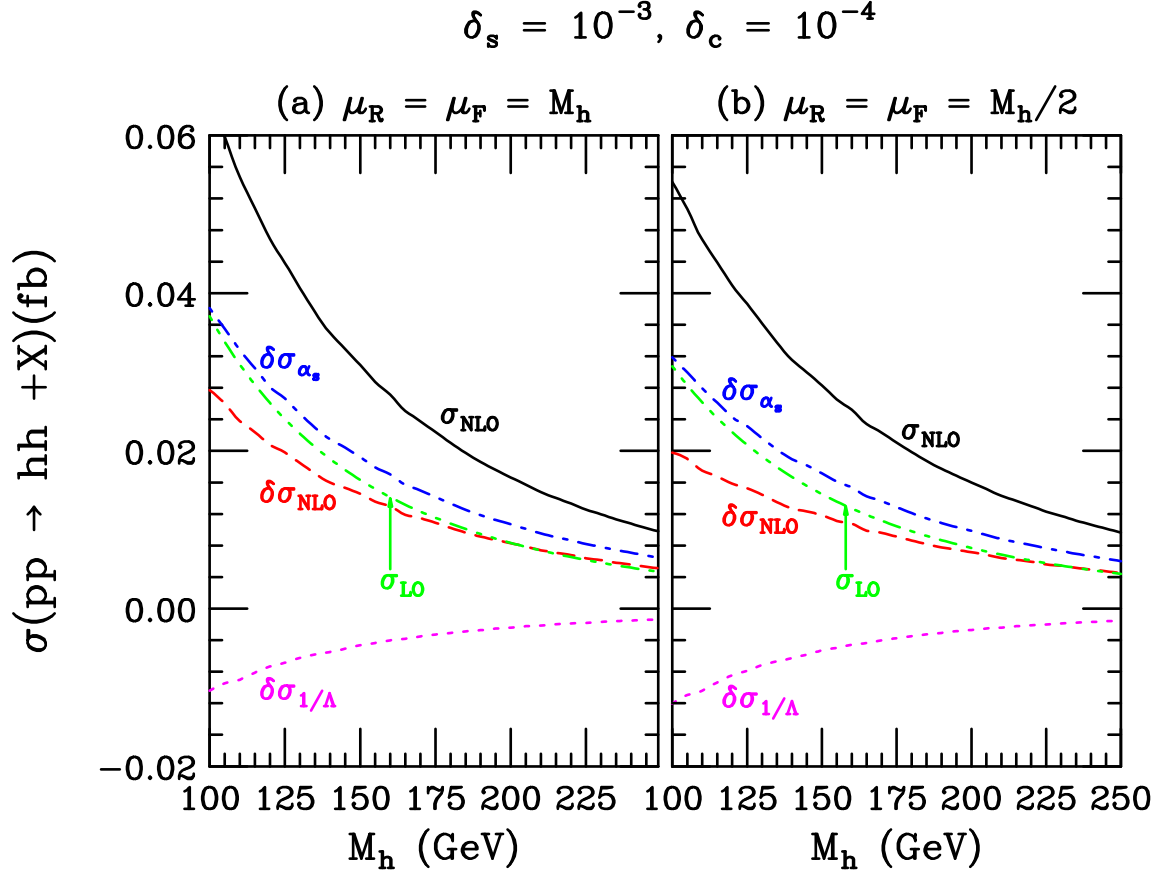
18

FIG. 9: Next-to-leading order cross section $\sigma_{NLO}(pp \to hh + X)$ (solid, black) in bottom quark fusion versus the Higgs mass (M_h) with $\sqrt{S} = 14$ TeV, $\delta_s = 10^{-3}$ and $\delta_c = 10^{-4}$, for (a) $\mu_R = \mu_F = M_h$ and (b) $\mu_R = \mu_F = M_h/2$. Also shown are the LO cross section σ_{LO} (dash-dot-dot, green), α_s corrections $\delta\sigma_{\alpha_s}$ (dash-dot, blue), $1/\Lambda$ corrections $\delta\sigma_{1/\Lambda}$ (dot, magenta), and the NLO correction $\delta\sigma_{NLO} = \delta\sigma_{\alpha_s} + \delta\sigma_{1/\Lambda}$ (dash, red).

In Fig. 10, we show the LO and the NLO cross section including the $\mathcal{O}(\alpha_s)$ contributions from the $b\bar{b}$ initial state and the $\mathcal{O}(1/\Lambda)$ contribution from the bg initial state. We separately show the $\mathcal{O}(1/\Lambda^2)$ contribution via $gg \to b\bar{b}hh$ as a function of the Higgs mass (M_h) at the LHC with $\sqrt{s} = 14$ TeV. As in Fig. 9, we present our results at two renormalization/factorization scales, (a) $\mu = M_h$ and (b) $\mu = M_h/2$ with $\delta_s = 10^{-3}$ and $\delta_c = 10^{-4}$.

In calculating the sub-leading contribution from the subprocess $gg \to b\bar{b}hh$, we have evaluated the cross section numerically for $pp \to b\bar{b}hh + X$ via $gg \to b\bar{b}hh$ with a finite quark mass to regulate the collinear singularity. We take the b quark mass to be $m_b = 4.7$ GeV.

As is shown in Fig. 10, both the LO and NLO total cross section for the $bb \to hh$ process at a renormalization/factorization scale M_h are bigger than the corresponding cross sections at the scale $M_h/2$.

In the Standard Model, gluon fusion is the dominant source for producing a pair of Higgs bosons through triangle and box diagrams containing top and bottom quark loops. It has been demonstrated that it might be possible to study the trilinear Higgs coupling at the LHC through the gluon fusion production mechanism of Higgs boson pairs [5, 6, 7, 8, 9]. In
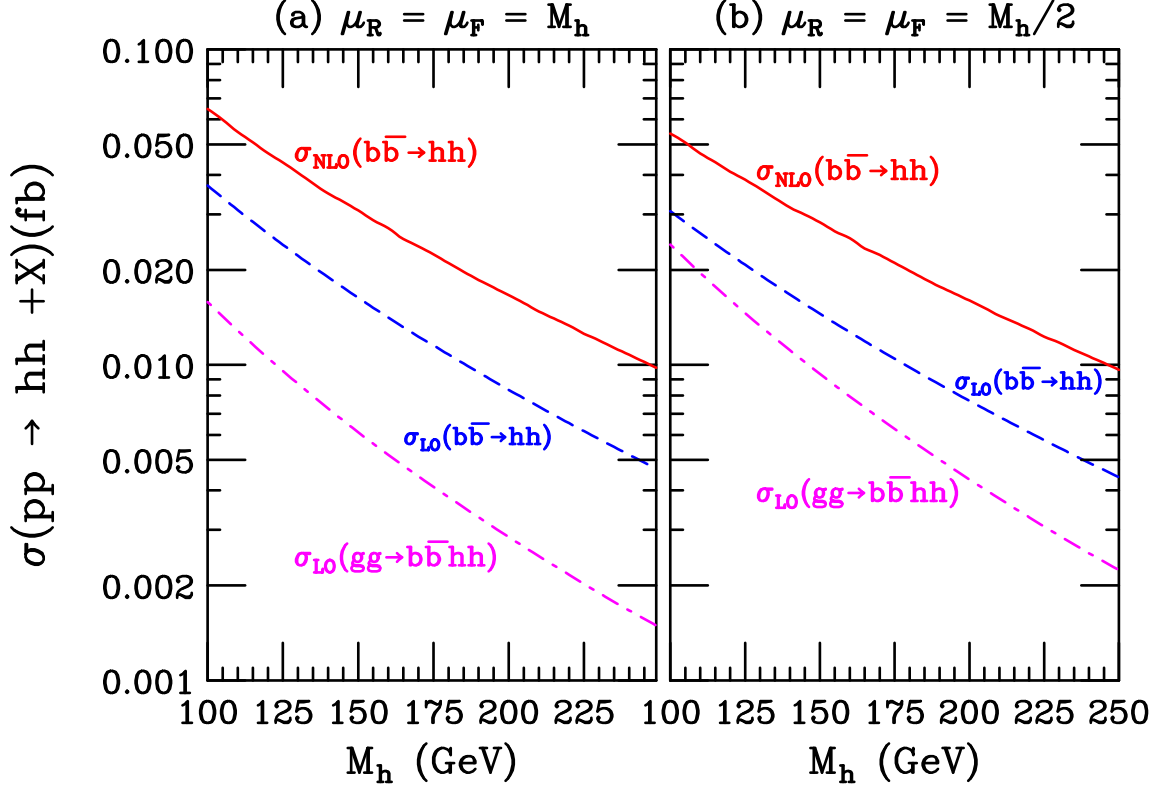
FIG. 10: Leading order cross section σ_{LO} (dash, blue) and next-to-leading order cross section σ_{NLO} (solid, red) for $pp \to hh + X$ via bottom quark fusion as a function of M_h at the LHC with $\sqrt{S} = 14$ TeV for (a) $\mu = M_h$ and (b) $\mu = M_h/2$. Also shown is the $\mathcal{O}(1/\Lambda^2)$ contribution from $gg \to b\bar{b}hh$.

the minimal supersymmetric standard model, bottom quark fusion could offer great promise to study the trilinear couplings of Higgs bosons for large values of $\tan\beta$ through $b\bar{b} \to hh$.

In Figure 11, we show the cross section for $pp \to hh + X$ via gluon fusion ($gg \to hh$) through top and bottom loop diagrams as a function of M_h at LHC with $\sqrt{S} = 14$ TeV for (a) $\mu = M_h$ and (b) $\mu = M_h/2$. In the SM this production mechanism is significantly larger than the $b\bar{b}$ fusion mechanism.

V. CONCLUSIONS

In this paper we present complete $\mathcal{O}(\alpha_s)$ and $\mathcal{O}(1/\Lambda)$ QCD corrections to the production of a pair of Higgs bosons via bottom quark fusion at the LHC. We introduce two arbitrary small cutoffs, δ_s and δ_c, to compute $\mathcal{O}(\alpha_s)$ NLO soft, hard/collinear and hard/non-collinear gluon emission corrections to $b\bar{b} \to hh$. The total $\mathcal{O}(\alpha_s)$ NLO cross section corrections are independent of the values of δ_s and δ_c.

Our results are not sensitive to the difference between renormalization and factorization scales and we use the same renormalization and factorization scales. The LO cross section is very sensitive to the factorization scale. The cross section for the $b\bar{b} \to hh$ process with
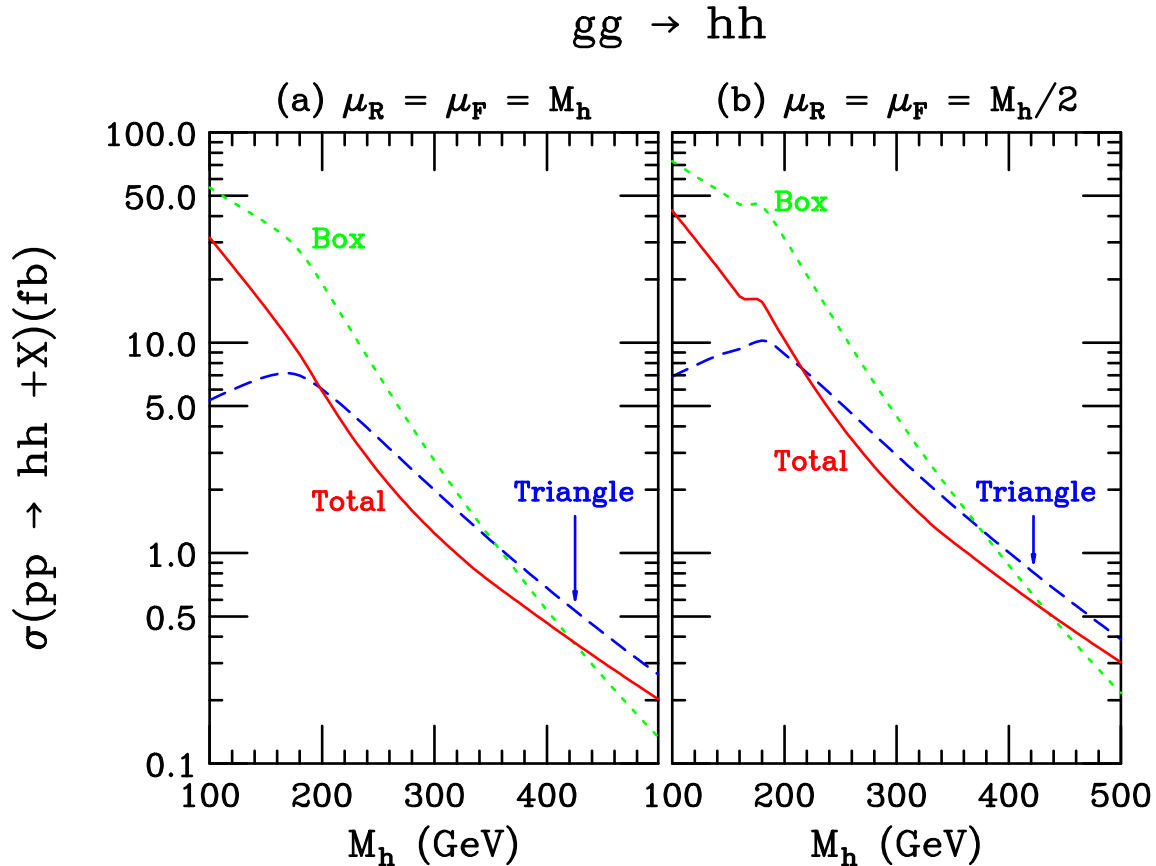
20

FIG. 11: Cross section of $pp \rightarrow hh + X$ via gluon fusion versus the Higgs mass (M_h) at LHC with $\sqrt{S} = 14$ TeV for the contributions from the triangle diagrams (dash, blue) and the box diagrams (dot, green) respectively. Also shown is the total cross section (solid). The renormalization and factorization scales are chosen to be (a) $\mu_R = \mu_F = M_h$ and (b) $\mu_R = \mu_F = M_h/2$.

large factorization scale is larger than the corresponding cross section with a low factorization scale.

The rate for double Higgs production in the SM is very small, although the NLO corrections we have computed significantly increase this rate. However, the rate for Higgs pair production will be enhanced in models with large couplings of the Higgs bosons to b quarks. Our results are of interest in attempts to measure the trilinear Higgs coupling in such models.

Acknowledgments

APPENDIX A: HEAVY QUARK RUNNING MASS

The two-loop running mass of a heavy quark in the $\overline{MS}$ scheme has the expression [17, 25]

$$\bar{m}(\mu) = \bar{m}(\mu_0) \left(\frac{\alpha_s(\mu)}{\alpha_s(\mu_0)} \right)^{\gamma_0/\beta_0} \frac{\left[1 + a_1 \frac{\alpha_s(\mu)}{\pi} + (a_1^2 + a_2)/2 \left(\frac{\alpha_s(\mu)}{\pi} \right)^2 \right]}{\left[1 + a_1 \frac{\alpha_s(\mu)}{\pi} + (a_1^2 + a_2)/2 \left(\frac{\alpha_s(\mu)}{\pi} \right)^2 \right]} \tag{A1}$$

where

$$
\begin{aligned}
a_1 &= -\frac{\beta_1 \gamma_0}{\beta_0^2} + \frac{\gamma_1}{\beta_0} \\
a_2 &= \frac{\gamma_0}{\beta_0^2} \left(\frac{\beta_1^2}{\beta_0} - \beta_2 \right) - \frac{\beta_1 \gamma_1}{\beta_0^2} + \frac{\gamma_2}{\beta_0} \\
\gamma_0 &= 1 \\
\gamma_1 &= \frac{1}{16} \left(\frac{202}{3} - \frac{20}{9} N_f \right) \\
\gamma_2 &= \frac{1}{64} \left[1249 + \left(-\frac{2216}{27} - \frac{160}{3} \zeta_3 \right) N_f - \frac{140}{81} N_f^2 \right] \\
\beta_0 &= \frac{1}{4} \left(11 - \frac{2}{3} N_f \right) \\
\beta_1 &= \frac{1}{16} \left(102 - \frac{38}{3} N_f \right)
\end{aligned}
\tag{A2}
$$

where N_f is the number of quark flavors with mass less than $\mu(\mu > \mu_0)$, and ζ is the Riemann zeta function with $\zeta_3 = 1.2020569$.

The $\overline{MS}$ mass at next-leading order is

$$M_Q = \bar{m}(M_Q) \left(1 + C_F \frac{\alpha_s}{\pi} \right) \tag{A3}$$

Here M_Q is the heavy quark pole mass. The evolution of the strong coupling can be found in Ref. [26].

---

[1] R. Barate *et al.*, [LEP Working Group for Higgs boson searches], Phys. Lett. B **565**, 61 (2003) [arXiv:hep-ex/0306033].

[2] The LEP Electroweak Working Group for the LEP Collaborations, [arXiv:hep-ex/0511027].

[3] The LEP Electroweak Working Group, http://lepewwg.web.cern.ch/LEPEWWG/.

[4] D. Glenzinski *et al.*, Tevatron Electroweak Working Group for the CDF and D0 Collaborations, [ArXiv: hep-ex/0608032].

[5] F. Boudjema and E. Chopin, Z. Phys. C **73**, 85 (1996) [arXiv:hep-ph/9507396].

[6] A. Djouadi, W. Kilian, M. Muhlleitner and P. M. Zerwas, Eur. Phys. J. C **10**, 45 (1999) [arXiv:hep-ph/9904287].

[7] M. Muhlleitner and M. Spira, Phys. Rev. D **68**, 117701 (2003).

[8] U. Baur, T. Plehn and D. L. Rainwater, Phys. Rev. D **69**, 053004 (2004) [arXiv:hep-ph/0310056].

[9] M. Moretti, S. Moretti, F. Piccinini, R. Pittau and A. D. Polosa, JHEP **0502**, 024 (2005) [arXiv:hep-ph/0410334].

[10] D. A. Dicus, C. Kao and S. S. D. Willenbrock, Phys. Lett. B **203**, 457 (1988).

[11] E. W. N. Glover and J. J. van der Bij, Nucl. Phys. B **309**, 282 (1988).

[12] S. Dawson, S. Dittmaier and M. Spira, Phys. Rev. D **58**, 115012 (1998) [arXiv:hep-ph/9805244].

[13] A. A. Barrientos Bendezu and B. A. Kniehl, Phys. Rev. D **64**, 035006 (2001) [arXiv:hep-ph/0103018].

[14] F. I. Olness and W. K. Tung, Int. J. Mod. Phys. A **2**, 1413 (1987).

[15] R. M. Barnett, H. E. Haber and D. E. Soper, Nucl. Phys. B **306**, 697 (1988).

[16] T. Stelzer, Z. Sullivan and S. Willenbrock, Phys. Rev. D **58**, 094021 (1998) [arXiv:hep-ph/9807340].

[17] D. Dicus, T. Stelzer, Z. Sullivan and S. Willenbrock, Phys. Rev. D **59**, 094016 (1999) [arXiv:hep-ph/9811492].

[18] L. G. Jin, C. S. Li, Q. Li, J. J. Liu and R. J. Oakes, Phys. Rev. D **71**, 095004 (2005) [arXiv:hep-ph/0501279].

[19] A. Hocker, DØ results presented at the 33rd International Conference on High Energy Physics (ICHEP06) in Moscow, Russia, July 26 - August 2, 2006.

[20] S. Dawson, C. Kao, and Y. Wang, in preparation.

[21] J. Ohnemus and J. F. Owens, Phys. Rev. D **43**, 3626 (1991).

[22] B. W. Harris and J. F. Owens, Phys. Rev. D **65**, 094032 (2002) [arXiv:hep-ph/0102128].

[23] MADGRAPH, by T. Stelzer and W.F. Long, Comput. Phys. Commun. **81**, 357 (1994); F. Maltoni and T. Stelzer, JHEP **0302**, 027 (2003) [arXiv:hep-ph/0208156].

[24] HELAS, by H. Murayama, I. Watanabe and K. Hagiwara, KEK report KEK-91-11 (1992).

[25] J. A. M. Vermaseren, S. A. Larin and T. van Ritbergen, Phys. Lett. B **405**, 327 (1997) [arXiv:hep-ph/9703284].

[26] W. J. Marciano, Phys. Rev. D **29**, 580 (1984).

[27] M. A. Aivazis, J. C. Collins, F. I. Olness and W. K. Tung, Phys. Rev. D **50**, 3102 (1994) [arXiv:hep-ph/9312319].

[28] J. C. Collins, Phys. Rev. D **58**, 094002 (1998) [arXiv:hep-ph/9806259].

[29] M. Kramer, F. I. Olness and D. E. Soper, Phys. Rev. D **62**, 096007 (2000) [arXiv:hep-ph/0003035].

[30] L. Lewin, *Dilogarithms and Asscociated Functions*, Macdonald, London, (1958).

[31] E. Braaten and J. P. Leveille, Phys. Rev. D **22**, 715 (1980).

[32] J. Pumplin, D. R. Stump, J. Huston, H. L. Lai, P. Nadolsky and W. K. Tung, JHEP **0207**, 012 (2002) [arXiv:hep-ph/0201195].